Available online at www.sciencedirect.com
ScienceDirect
Journal of Solid State Chemistry 180 (2007) 1414–1420
JOURNAL OF SOLID STATE CHEMISTRY
www.elsevier.com/locate/jssc

High-temperature thermoelectric studies of $A_{11}Sb_{10}$ (A = Yb, Ca)

Shawna R. Brown[a], Susan M. Kauzlarich[a,*], Franck Gascoin[b,1], G. Jeffrey Snyder[b,**]

[a]*Department of Chemistry, University of California, One Shields Avenue, Davis, CA 95616, USA*
[b]*California Institute of Technology, 1200 California Boulevard, Pasadena, CA 91125, USA*

Received 21 December 2006; received in revised form 10 February 2007; accepted 12 February 2007
Available online 21 February 2007

Abstract

Large samples (6–8 g) of $Yb_{11}Sb_{10}$ and $Ca_{11}Sb_{10}$ have been synthesized using a high-temperature (1275–1375 K) flux method. These compounds are isostructural to $Ho_{11}Ge_{10}$, crystallizing in the body-centered, tetragonal unit cell, space group $I4/mmm$, with $Z = 4$. The structure consists of antimony dumbbells and squares, reminiscent of Zn_4Sb_3 and filled Skutterudite (e.g., $LaFe_4Sb_{12}$) structures. In addition, these structures can be considered Zintl compounds; valence precise semiconductors with ionic contributions to the bonding. Differential scanning calorimetry (DSC), thermogravimetry (TG), resistivity (ρ), Seebeck coefficient (α), thermal conductivity (κ), and thermoelectric figure of merit (zT) from room temperature to at minimum 975 K are presented for $A_{11}Sb_{10}$ (A = Yb, Ca). DSC/TG were measured to 1400 K and reveal the stability of these compounds to ~1200 K. Both $A_{11}Sb_{10}$ (A = Yb, Ca) materials exhibit remarkably low lattice thermal conductivity (~10 mW/cm K for both $Yb_{11}Sb_{10}$ and $Ca_{11}Sb_{10}$) that can be attributed to the complex crystal structure. $Yb_{11}Sb_{10}$ is a poor metal with relatively low resistivity (1.4 mΩ cm at 300 K), while $Ca_{11}Sb_{10}$ is a semiconductor suggesting that a gradual metal–insulator transition may be possible from a $Ca_{11-x}Yb_xSb_{10}$ solid solution. The low values and the temperature dependence of the Seebeck coefficients for both compounds suggest that bipolar conduction produces a compensated Seebeck coefficient and consequently a low zT.

Keywords: High-temperature thermoelectric; Zintl compounds; Binary antimonide; Figure of merit; Thermal conductivity; Electrical resistivity; Seebeck coefficient

1. Introduction

High-temperature thermoelectric materials are becoming increasingly useful for applications such as power generation of deep space probes, sea buoys and remote telecommunications. Generators engineered from these materials are environmentally benign power sources that could provide part of the solution to today's energy problems. These generators convert thermal energy directly into electrical energy, require little to no fuel, minimal maintenance and can be segmented to operate over a large temperature range (300–1275 K). They also produce negligible emissions and are virtually noise free.

The performance of a thermoelectric material is primarily a function of the dimensionless figure of merit (zT). Here, $zT = \alpha^2 T/\rho\kappa_T$ (α, Seebeck coefficient (μV/K); T, temperature (K); ρ, electrical resistivity (mΩ cm); κ_T, thermal conductivity (mW/cm K)) [1]. Hence, for promising thermoelectric compounds, the values for the electrical resistivity and thermal conductivity must be low and the Seebeck coefficient must be large, such has been seen in the antimonides, Zn_4Sb_3 and the filled Skutterudite (e.g., $LaFe_4Sb_{12}$) phases [1–6].

Zn_4Sb_3 possesses low thermal conductivity due to its complex structure, containing both $[Sb_2]^{4-}$ dumbbells and Sb^{3-} anions as well as disordered zinc atoms [5]. The simpler filled Skutterudite structure, containing the polyatomic Zintl $[Sb_4]^{4-}$ anion, has somewhat higher lattice thermal conductivity [3,4,6]. Zn_4Sb_3 with its remarkably low thermal conductivity shows high zT at temperatures greater than 600 K [7]. We are targeting chemically similar compounds with even more structural complexity in order

*Corresponding author. Fax: +1 530 752 8995.
**Corresponding author.
E-mail address: smkauzlarich@ucdavis.edu (S.M. Kauzlarich).
[1]Current address: Laboratoire de Physico-Chimie de la Matière Condensée, Université Montpellier 2, Place Eugène Bataillon, 34095 Montpellier Cedex 5, France.

0022-4596/$ - see front matter © 2007 Elsevier Inc. All rights reserved.
doi:10.1016/j.jssc.2007.02.007

to obtain a low lattice thermal conductivity. A recent successful example of this approach is the high-efficiency thermoelectric compound, $Yb_{14}MnSb_{11}$ [8].

Two binary Zintl compounds, $A_{11}Sb_{10}$ (A = Yb, Ca) have been synthesized and possess promising thermoelectric traits [9], that could potentially lead to the discovery of improved thermoelectric device efficiencies [10–14]. $Yb_{11}Sb_{10}$ is isostructural to $Ho_{11}Ge_{10}$, crystallizing in the body-centered, tetragonal unit cell, space group $I4/mmm$, with $Z = 4$ [13]. $Ca_{11}Sb_{10}$, discovered by Deller and Eisenmann in 1976, was reported to be of the $Yb_{11}Sb_{10}$ structure type [12] (or, more appropriately, of the $Ho_{11}Ge_{10}$ structure type). $Yb_{11}Sb_{10}$ can be described as containing two $[Sb_4]^{4-}$ anionic squares, eight $[Sb_2]^{4-}$ anionic dumbbells, 16 Sb^{3-} anions and 44 Yb^{2+} cations within each unit cell [15]. Fig. 1 shows two perspective views of $A_{11}Sb_{10}$ (A = Yb, Ca): along the c-axis and along the b-axis. The green and purple spheres represent the Yb/Ca and Sb, respectively. The $A_{11}Sb_{10}$ structure contains structural resemblances with Zn_4Sb_3 and filled Skutterudites (Zn_4Sb_3 contains Sb dumbbells [5], and antimony Skutterudites contain Sb_4 squares [16]) all of which adds motivation for this study. In addition, the $A_{11}Sb_{10}$ compounds are considered to be Zintl phases [17] and are expected to possess semiconducting electronic properties suitable for thermoelectrics. The Zintl description considers the cations to be ionically bonded with isolated Sb anions, Sb_2 dumbbells, and Sb_4 square planar rings.

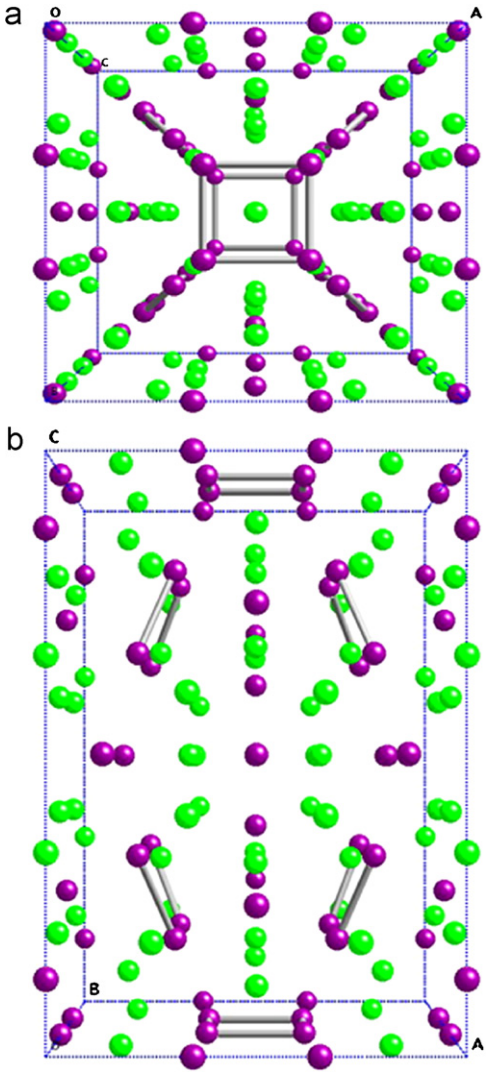

Fig. 1. Body-centered, $I4/mmm$ crystal structure of $A_{11}Sb_{10}$ (A = Yb, Ca). The green and purple spheres represent Yb/Ca and Sb, respectively. (a) View along the c-axis, illustrating the anionic squares. (b) View along the b-axis, illustrating the antimony dumbbells.

Indeed, our interest in the $A_{11}Sb_{10}$ system was motivated not only by its similar structural complexity to materials showing notable thermoelectric properties [5,7,16], but also because these two compounds possess a number of traits that typically provide good thermoelectric behavior. In particular, the presence of a small band gap, a large unit cell, and heavy main group elements [9]. Moreover, because this structure can be easily modified by cation and/or anion substitution, there is the potential for optimization of the thermoelectric parameters through the synthesis of a solid solution.

This paper presents differential scanning calorimetry/thermogravimetry (DSC/TG), electrical resistivity, Seebeck coefficient, Hall effect, thermal conductivity and thermoelectric figure of merit from room temperature to at minimum 975 K for $Yb_{11}Sb_{10}$ and $Ca_{11}Sb_{10}$. The results are compared with Zn_4Sb_3 and the filled Skutterudite phases. In addition, suggestions for optimization of the thermoelectric parameters are provided.

2. Experimental procedure

2.1. $A_{11}Sb_{10}$ (A = Yb, Ca)

2.1.1. Synthesis

Sublimed dendritic Yb metal (Alfa Aesar, 99.99%) and Ca metal (Alfa Aesar, 99.987%) were cut into small pieces. Sb pieces (Allied Chemical, 99.7%) and Sn granules (Mallinkrodt, 99.967%) were used as received. All materials were handled in a nitrogen-filled drybox with water levels below 1.0 ppm. Both of the $A_{11}Sb_{10}$ (A = Yb, Ca) phases were prepared by way of a Sn-flux method with techniques similar to those stated by Canfield and Fisk for the CeSb system [18]. The elements Yb:Sb:Sn and Ca:Sb:Sn were layered in 2 and 5 cm^3 Al_2O_3 crucibles in the ratios of 11:10:79 and 11:10:50, respectively. The reactions were sealed in quartz ampoules under 1/5 atm argon atmosphere, placed in high-temperature programmable furnaces, and brought up to maximum temperatures of 1375 K for $Yb_{11}Sb_{10}$ and 1275 K for $Ca_{11}Sb_{10}$ following a similar ramp-up procedure as described by Fisher et al. [19]. Once at maximum temperatures, the reactions were held for 1 h, and then cooled at a rate of 275 or 277 K/h to 1075 K for $Yb_{11}Sb_{10}$ and 975 K for $Ca_{11}Sb_{10}$. Upon reaching final temperatures, the reactions were inverted and spun in a centrifuge to separate the molten Sn-flux from the single-crystal products. Moderate yields

(40–60%) of reflective, silver colored single-crystal ingots were obtained. All reactions were opened and examined in a nitrogen-filled drybox equipped with a microscope and water levels below 1.0 ppm. $Yb_{11}Sb_{10}$ and $Ca_{11}Sb_{10}$ are both air and water sensitive and the crystals slowly degrade upon exposure to air and moisture. $Ca_{11}Sb_{10}$ degrades more rapidly than $Yb_{11}Sb_{10}$ and the crystals visibly change from highly reflective silver color to dull black within a few minutes.

2.1.2. X-ray powder diffraction

While in a nitrogen-filled drybox, $Yb_{11}Sb_{10}$ and $Ca_{11}Sb_{10}$ crystals were inspected, ground into a fine powder, and placed in an air-sensitive sample holder. Phase identification was completed by way of X-ray powder diffraction (XRD) using an Inel diffractometer, XRG 3000 ($CoK\alpha_1$ radiation). Patterns were acquired from 0° to 120° 2θ at a 10° incident angle. The data were analyzed and refined for lattice parameters using MDI JADE 6.5 [20]. Data were also collected on a Siemens D500 diffractometer. The calculated diffraction patterns were generated from the reported crystal structures [12,13] and produced using Crystal Maker 7.1 [21].

2.1.3. Differential scanning calorimetry and thermogravimetry measurements (DSC/TG)

A Netzsch Thermal Analysis STA 409 cell, equipped with a TASC 414/2 controller and PU 1.851.01 power unit, was used to evaluate the thermal properties of $Yb_{11}Sb_{10}$ and $Ca_{11}Sb_{10}$ between 298 and 1400 K. After a baseline was established, finely ground samples (80–100 mg) were placed in Al_2O_3 crucibles and heated at 10 K/min under flowing argon with an acquisition rate of 2.0 pts/K. Data were acquired using the software provided with the instrument. Analysis was performed using Netzsch Proteus Analysis.

2.1.4. Thermoelectric properties sample preparation

In order to acquire a dense sample, the finely ground polycrystalline powder was hot-pressed in high-density graphite dies (POCO). A cylinder about 5.9 mm long and 12 mm in diameter was obtained. Its density (calculated from measured dimensions and weight) was found to be about 95% of the theoretical density. The hot-pressing was conducted at a pressure of ~20,000 psi and 1073 K for 1.5 h under argon atmosphere.

Samples were sliced (typically 1 mm thick and 12 mm diameter) from the hot-pressed cylinder using a diamond saw and were used to measure the electrical and thermal transport properties. The Seebeck coefficient measurement was performed on the remaining cylinder. All physical properties were measured between room temperature and 1075 K.

2.1.5. Resistivity measurements

Electrical resistivity (ρ) was measured by way of the van der Pauw technique using a current of 100 mA and a special high-temperature apparatus [22].

2.1.6. Hall coefficient measurements

The Hall coefficient was measured in the same apparatus as the resistivity with a constant magnetic field value of about 10,100 G. The carrier density was calculated from the Hall coefficient (R_H) (assuming a scattering factor of 1.0 in a single carrier scheme) by n or $p = 1/R_H e$, where p and n are the densities of holes and electrons, respectively, and e is the charge of the electron. The Hall mobility (μ_H) was calculated from the Hall coefficient and the resistivity values with $\mu_H = R_H/\rho$.

2.1.7. Thermal conductivity measurements

The thermal diffusivity and heat capacity of $Yb_{11}Sb_{10}$ were measured by a laser flash technique in a Netzsch LFA 457 system in dynamic vacuum using a pyroceram standard for heat capacity measurements. The heat capacity was found to be close to the Dulong–Petit (0.168 J/g K) value with a slight, linear increase with temperature. A linear fit to the heat capacity and the experimental density was used to calculate the thermal conductivity from the thermal diffusivity measurements. The thermal diffusivity of $Ca_{11}Sb_{10}$ was measured using a flash diffusivity technique [23]. The thermal conductivity (λ) was then calculated from the experimental density, the Dulong–Petit ($3k_b$/atom) value for the heat capacity, and thermal diffusivity measurements. The Lorenz factor typical for metals ($2.4 \times 10^{-8}\,J^2/K^2\,C^2$) is used to estimate the electronic contribution to the thermal conductivity, $\kappa_E = LT/\rho$.

2.1.8. Seebeck measurements

The Seebeck coefficient (α) was measured using a high-temperature light pulse technique using W/Nb thermocouples [24].

3. Results and discussion

3.1. Characterization

Large crystals of the two compounds were prepared via flux synthesis. Their structure was verified with powder X-ray diffraction and the crystals were ground into a powder for hot-pressing. X-ray diffraction patterns taken before and after hot-pressing show little or no decomposition of the compound. Fig. 2 compares the experimentally obtained powder diffraction patterns (upper plots) with patterns calculated from published crystallographic structures (lower plots) for $Yb_{11}Sb_{10}$ and $Ca_{11}Sb_{10}$ [12,13]. There is a good match to the calculated powder diffraction patterns for both materials with only a couple unindexed peaks. The unindexed peaks are marked with an asterisk. The best match to the one unindexed peak for $Yb_{11}Sb_{10}$ is Yb_2O_3 [26], presumably from a slight oxidation of the sample. The refined cell for $Yb_{11}Sb_{10}$ resulted in the room temperature lattice parameters of $a = 11.900(1)$ Å and $c = 17.156(2)$ Å, with a volume of 2429.42(1) Å^3 and density of 8.53 g/cm^3 giving rise to a 2.97% ESD of fit. The two unindexed peaks for $Ca_{11}Sb_{10}$ correlate best with

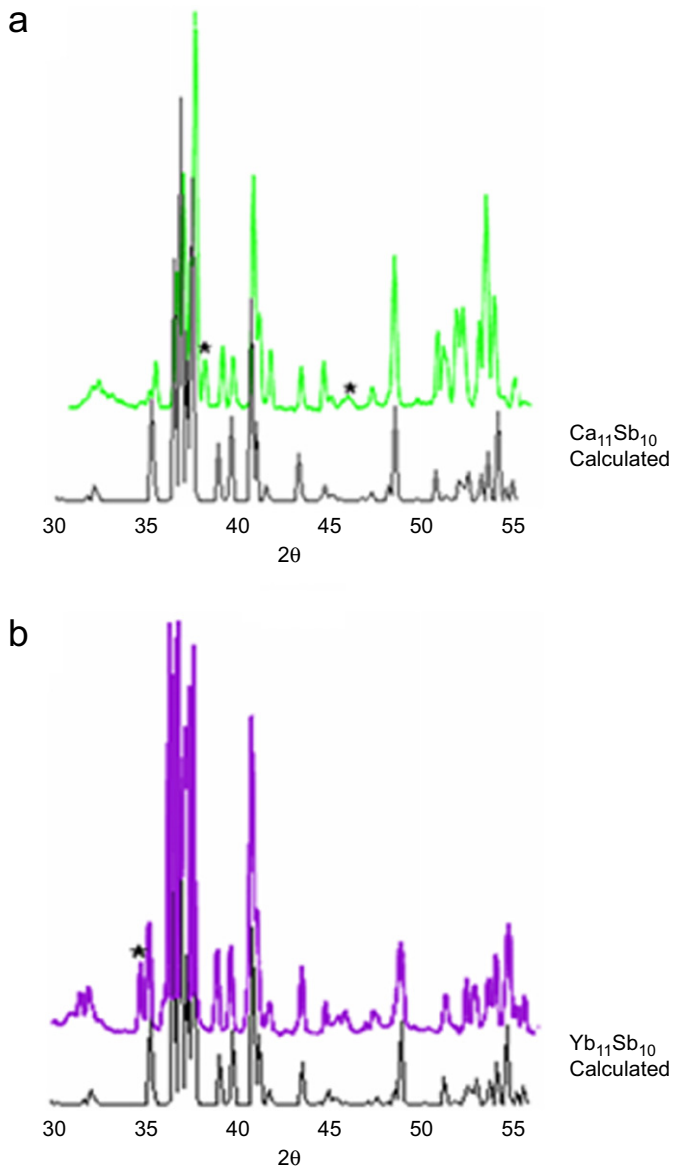

Fig. 2. X-ray powder diffraction of (a) $Ca_{11}Sb_{10}$ and (b) $Yb_{11}Sb_{10}$. In each plot, the upper data are experimentally determined and the lower data are calculated.

the binary phase Ca_5Sb_3 [25]. Cell refinement for $Ca_{11}Sb_{10}$ provided room temperature lattice parameters of $a = 11.701(1)$ Å and $c = 17.190(1)$ Å with volume of 2353.37(1) Å^3 and density of 4.68 g/cm^3, resulting in a 7.88% ESD of fit. Both refinements give lattice parameters that correlate well with published values [12,13]. While the flux synthesis method results in high-quality, large crystals that are free from impurities, in order to prepare samples of sufficient size, the crystals were ground together, resulting in a slight contamination from some Sn-flux remaining on the surface of some of the crystals. Small amounts of impurities can also be present on the surface. However, the additional phases must be fairly small, as they do not appear to greatly affect the thermal or electronic properties described below.

3.1.1. Properties measurements

Differential scanning calorimetry (DSC) and thermogravimetry (TG) results indicate that the compounds, $Yb_{11}Sb_{10}$ and $Ca_{11}Sb_{10}$, are stable to at least ~1200 K under flowing argon. Figs. 3a and 3b illustrate the DSC (upper plot with arrows) and TG (lower plot) measurements for $Yb_{11}Sb_{10}$ and $Ca_{11}Sb_{10}$, respectively. The data show a small exotherm at ~500 K, indicating a minimal amount of remnant Sn-flux. Both materials appear to exhibit sintering upon heating, as is depicted by the continual slight increase in DSC data upon heating with no accompanying weight loss or gain. It is evident that neither material reaches a melting point to ~1200 K. For $Yb_{11}Sb_{10}$, the DSC data reveal a two-stepped exotherm near 1300 K. This exotherm can be interpreted as evidence for the α–β phase change indicated in the Sb–Yb phase diagram [11], and then melting of the material. Upon cooling, only one phase recrystallizes. The TG data for $Yb_{11}Sb_{10}$ show no weight loss or gain to 1300 K indicating

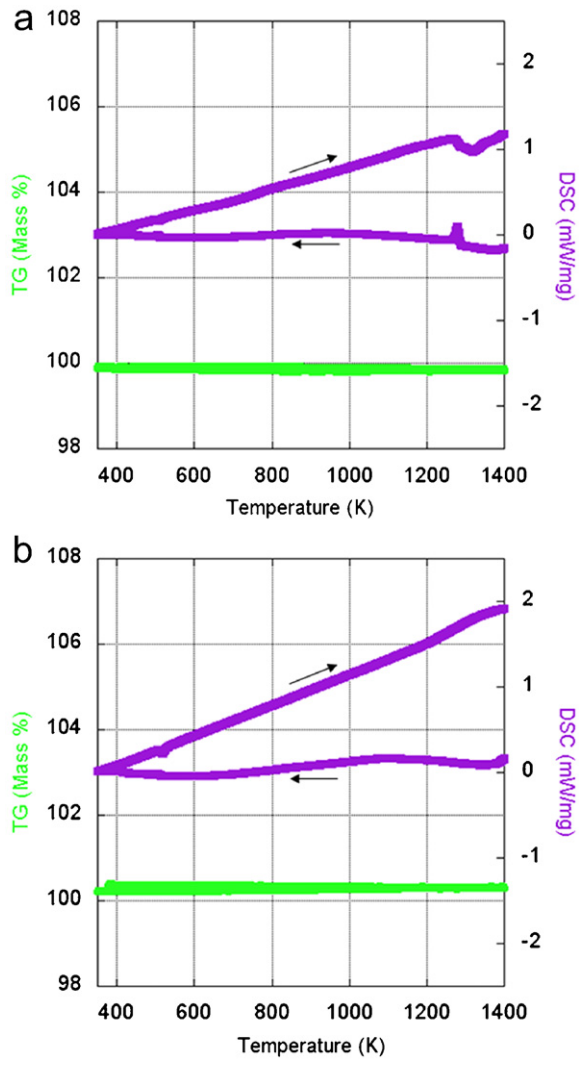

Fig. 3. Differential scanning calorimetry (DSC) and thermogravimetry (TG) of (a) $Yb_{11}Sb_{10}$ and (b) $Ca_{11}Sb_{10}$. $Yb_{11}Sb_{10}$ data are represented by purple open circles and $Ca_{11}Sb_{10}$ data are represented by green squares.

no loss of antimony or of ytterbium or oxidation of the sample under argon atmosphere. DSC data for $Ca_{11}Sb_{10}$ show that the material is stable to ~1400 K. The TG data remains constant throughout the measurement (300–1275 K) illustrating that there was no decomposition or oxidation occurring.

The electrical properties of $Yb_{11}Sb_{10}$ (open circles) and $Ca_{11}Sb_{10}$ (filled squares) are presented in Fig. 4. Fig. 4a shows that the resistivity for $Yb_{11}Sb_{10}$ slightly increases from 300 to 500 K (~1.25–1.4 mΩ cm), leveling out at 1.4 mΩ cm and then remaining constant to 1000 K. This value is in the range of a good thermoelectric material (~1 mΩ cm). The resistivity for $Ca_{11}Sb_{10}$ decreases quickly with increasing temperature reaching ~3 mΩ cm at 1150 K.

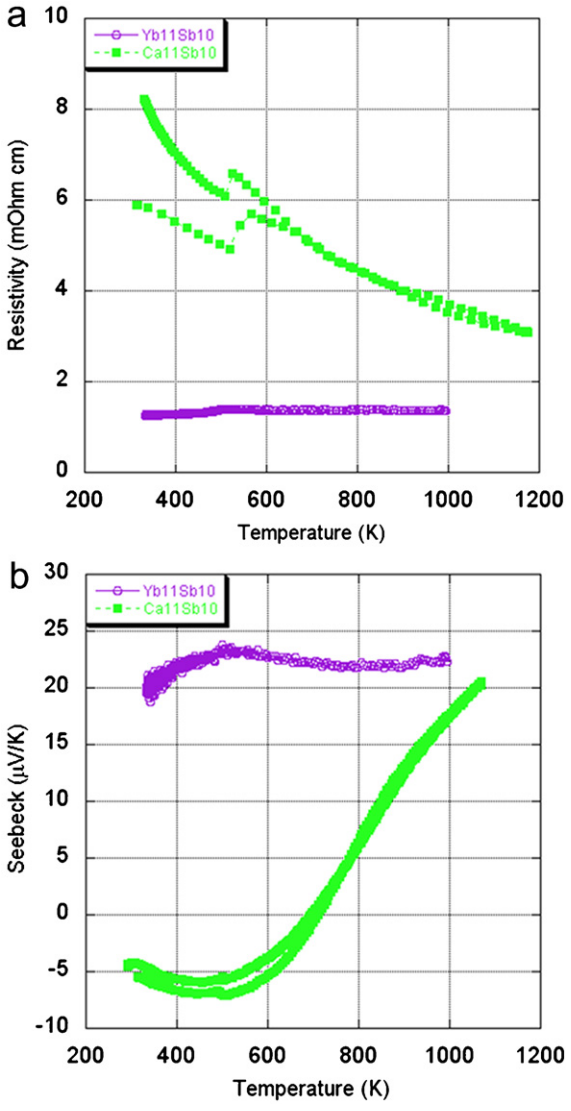

Fig. 4. (a) Resistivity of $Yb_{11}Sb_{10}$ (purple circles) and $Ca_{11}Sb_{10}$ (green squares) resulting in high temperature values of 1.4 and 3 mΩ cm at 1000 and 1150 K, respectively. Double lines represent heating and cooling scans. (b) Seebeck coefficient for $Yb_{11}Sb_{10}$ (circles) and $Ca_{11}Sb_{10}$ (squares) reaching maximum values of +23 and +20 mV/K at 1000 and 1100 K, respectively, indicating p-type behavior for both materials. Plots include both heating and cooling data.

Both samples show a transition at ~500 K (same temperature as the transition seen in the DSC data), which can be attributed to remnant Sn-flux. The effect is significant for $Ca_{11}Sb_{10}$ and barely observable for $Yb_{11}Sb_{10}$. The mobility of both samples is low making the measurements difficult. $Yb_{11}Sb_{10}$ appears to have a p-type mobility of about 2 $cm^2/V\,s$ which implies a carrier concentration of about $1 \times 10^{21}\,cm^{-3}$. The Hall mobility of $Ca_{11}Sb_{10}$ is less than 2 $cm^2/V\,s$ and it is difficult to tell whether it is n- or p-type. Because the resistivity of $Ca_{11}Sb_{10}$ is more like an intrinsic semiconductor than $Yb_{11}Sb_{10}$, the Sn and any other impurities should have a larger effect on the electrical properties of $Ca_{11}Sb_{10}$.

The temperature-dependent resistivity of $Yb_{11}Sb_{10}$ has the slope of a poor metal, while $Ca_{11}Sb_{10}$ is clearly a semiconductor. Because both compounds have the same structure type and Yb and Ca have the same valence and similar size, it is expected that a $Ca_{11-x}Yb_xSb_{10}$ solid solution could be synthesized. The $Ca_{11-x}Sr_xSb_{10}$ solid solution has been reported and shows complex structural site preferences [10]. Resistivity was measured by the Q method over a range of 110–294 K [27] and indicate that the compounds $Ca_{5.5}Sr_{5.5}Sb_{11}$ and $Ca_{3.4}Sr_{7.5}Sb_{10}$ were non-metallic. If a solid solution such as $Ca_{11-x}Yb_xSb_{10}$ could be prepared, it may gradually transition from a metal to a semiconductor allowing careful tuning of the electronic properties, very similar to that found in the $Ca_{1-x}Yb_xZn_2Sb_2$ solid solution [28].

Fig. 4b reveals that the Seebeck coefficient for $Yb_{11}Sb_{10}$ (open circles) is consistent with the dominant carriers in the sample being holes, indicating p-type behavior; however, it does not increase with increasing temperature. Instead, the Seebeck coefficient remains constant at ~+23 μV/K, between the temperatures of 300 and 1000 K, which is unusual for simple metals or semiconductors. The Seebeck coefficient for $Ca_{11}Sb_{10}$ (filled squares) reveals a compensated thermopower due to competing n- and p-type carriers. At low temperatures, the n-type carriers dominate the Seebeck while at temperatures above 700 K the p-type carriers dominate.

The atypical electronic transport properties all point to a complex band structure with multiple carrier types coexisting. Theoretical calculations using molecular orbital and periodic tight binding method have been published for $M_{11}X_{10}$ (M = Sr, Ba; X = Sb, Bi) [14]. The anions can be considered isolated and for X_2^{4-}, the HOMO is degenerate (π_g) and corresponds to the p_yp_z nonbonding orbitals. The X_4^{4-} anion shows a large separation between the HOMO and LUMO confirming the stability of the square planar anion. The crystal orbital overlap populations (COOP) for different diatomic interactions show antibonding character near the Fermi level and with the cation–anion (M–X) bands consistent with bonding interaction [14]. Competing effects of n- and p-type carriers lead to low values for both Hall mobility and thermopower (absolute value of Seebeck) and a deviation of the typical temperature dependence expected from a single band, single carrier

type material. This is most obvious in $Ca_{11}Sb_{10}$ which shows a n-type Seebeck coefficient with n-type slope at room temperature, but at higher temperatures p-type carriers become activated and then dominate both the Seebeck and the Hall effect. Likewise, in $Yb_{11}Sb_{10}$, the presence of n-type carriers may be leading to the low thermopower that is not increasing significantly with temperature.

Total thermal conductivity data for $Yb_{11}Sb_{10}$ (open circles) and $Ca_{11}Sb_{10}$ (open squares) is shown in Fig. 5, along with the lattice thermal conductivity for $Yb_{11}Sb_{10}$ (closed circles). The total thermal conductivity of $Yb_{11}Sb_{10}$ increases with increasing temperature because of the large electronic contribution to the thermal conductivity which can be estimated by the Weidmann–Franz law relating the electronic conductivity to thermal conductivity. The thermal conductivity of $Ca_{11}Sb_{10}$ is almost entirely due to the lattice contribution because of its high electrical resistivity. The two compounds $Yb_{11}Sb_{10}$ and $Ca_{11}Sb_{10}$ have remarkably similar room temperature values and overall quite low lattice thermal conductivity. The lattice contribution to the thermal conductivity of both $A_{11}Sb_{10}$ compounds is only about 10 mW/cm K while that of SiGe alloys (current state-of-the-art high-temperature thermoelectric materials) is 30–40 mW/cm K [29]. This value is lower than that observed for the best filled Skutterudites [6] and comparable with Zn_4Sb_3. This greatly reduced value can be attributed to the complex crystal structure of $A_{11}Sb_{10}$, with multiple anion types, compared to the simple diamond structure of SiGe alloys. These results suggest that a $Ca_{11-x}Yb_xSb_{10}$ solid solution should result in even lower thermal conductivity due to disorder scattering of phonons as is seen in SiGe when compared to its pure elements, Si or Ge [29].

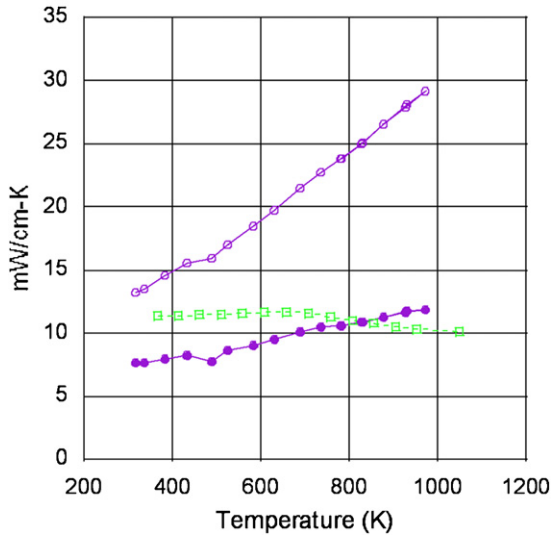

Fig. 5. Total thermal conductivity (mW/cm K) and lattice thermal conductivity of $Yb_{11}Sb_{10}$ (open purple circles and closed purple circles, respectively) and total thermal conductivity of $Ca_{11}Sb_{10}$ (open green squares). The $Yb_{11}Sb_{10}$ data results in total thermal conductivity of ~30 mW/cm K and lattice thermal conductivity of ~12 mW/cm K at 950 K. $Ca_{11}Sb_{10}$ results in a consistently low total thermal conductivity of ~10 mW/cm K between 300 and 1050 K.

For use as a thermoelectric material, the thermopower of the materials should be well over 100 μV/K [30]. This will require significant alteration of the electronic band structure so that only a single carrier type is present. With the low resistivity and low lattice thermal conductivity, there is some prospect for application of the $A_{11}Sb_{10}$ structure type for thermoelectrics, if a single carrier type material could be produced perhaps by selecting appropriate cation mixtures.

3.1.2. *Figure of merit*

Combining the electrical and thermal properties for $Yb_{11}Sb_{10}$ and $Ca_{11}Sb_{10}$ results in the dimensionless thermoelectric figure of merit. The maximum zTs for $Yb_{11}Sb_{10}$ and $Ca_{11}Sb_{10}$ are ~0.012 at 950 K and ~0.115 at 1050 K, respectively. Good thermoelectric materials tend to have phonon-glass, electron crystal transport properties [5]. $Yb_{11}Sb_{10}$ and $Ca_{11}Sb_{10}$ have remarkably low lattice thermal conductivities similar to phonon-glass type thermoelectric materials. The electronic properties indeed appear to be those of a (heavily doped) crystalline semiconductor. However, the bipolar nature of the conduction makes these materials unsuitable for thermoelectrics.

4. Summary

$Yb_{11}Sb_{10}$ and $Ca_{11}Sb_{10}$ have remarkably low lattice thermal conductivity similar to phonon-glass type thermoelectric materials. This can be attributed to the complex Zintl anions present, similar to those found in high thermoelectric figure of merit compounds, such as Zn_4Sb_3 [5], filled Skutterudites [16], and $Yb_{14}MnSb_{11}$ [8].

The electronic properties show both n- and p-type behavior, indicating that both carrier types are present resulting in low, compensated values for the Seebeck coefficient.

$Yb_{11}Sb_{10}$ is found to be a poor metal with relatively low resistivity (1.4 mΩ cm at 300 K), while $Ca_{11}Sb_{10}$ is a semiconductor suggesting that a gradual tuning of the metal–insulator transition is possible from a $Ca_{11-x}Yb_xSb_{10}$ solid solution. According to theoretical calculations, the more electropositive alkaline earth elements (i.e., Sr, Ba) in the A site increase the overlap populations [14]. Substituting larger alkaline earth elements into either the Yb or Ca system may provide an avenue into higher thermoelectric properties; although since there is site specificity [10], structure–property correlations may not be readily predictable.

In order to improve the electrical properties of these Zintl phases, an alteration of the band structure is needed to ensure that only one carrier type is present. This may be achieved through elemental substitutions that will affect the electronic band structure, such as adding some Ge or

Te for Sb or La or K for Yb and Ca. Efforts toward doping this phase to affect the electrical properties are underway.

Acknowledgments

We thank Japhe Rauscher for his assistance with XRD measurements. Portions of this work were carried out by the Jet Propulsion Laboratory, California Institute of Technology, under contract with NASA. This research is funded by NASA and NSF DMR-0600742.

References

[1] F.J. DiSalvo, Science 285 (1999) 703.
[2] H.J. Goldsmid, G.S. Nolas, in: Proceedings of the 20th International Conference on Thermoelectrics, 2001, p. 1.
[3] G.S. Nolas, M. Kaeser, R.T.I. Littleton, T.M. Tritt, Appl. Phys. Lett. 77 (2000) 1855.
[4] G.A. Lamberton Jr., S. Bhattacharya, R.T.I. Littleton, M.A. Kaeser, R.H. Tedstrom, T.M. Tritt, J. Yang, G.S. Nolas, Appl. Phys. Lett. 80 (2002) 598.
[5] G.J. Snyder, M. Christensen, E. Nishibori, T. Caillat, B.B. Iversen, Nat. Mater. 3 (2004) 458.
[6] G. Chen, M.S. Dresselhaus, G. Dresselhaus, J.-P. Fleurial, T. Caillat, Int. Mater. Rev. 48 (2003) 45.
[7] T. Caillat, J.P. Fleurial, A. Borshchevsky, J. Phys. Chem. Solids 58 (1997) 1119.
[8] S.R. Brown, S.M. Kauzlarich, F. Gascoin, G.J. Snyder, Chem. Mater. 18 (2006) 1873.
[9] G. Mahan, B. Sales, J. Sharp, Phys. Today 50 (1997) 42.
[10] S. Gupta, A.K. Ganguli, J. Solid State Chem. 179 (2006) 1924.
[11] V.D. Abulkhaev, Inorganic Materials (Translation of Neorganicheskie Materialy), vol. 35, 1999, p. 431.
[12] K. Deller, B. Eisenmann, Zeitsch. Naturforschung, Teil B: Anorgan. Chemie, Organ. Chemie 31B (1976) 29.
[13] H.L. Clark, H.D. Simpson, H. Steinfink, Inorg. Chem. 9 (1970) 1962.
[14] G. Derrien, M. Tillard-Charbonnel, A. Manteghetti, L. Monconduit, C. Belin, J. Solid State Chem. 164 (2002) 169.
[15] G.S. Smith, Q. Johnson, A.G. Tharp, Acta Crystallogr. 23 (1967) 640.
[16] J.W. Sharp, E.C. Jones, R.K. Williams, P.M. Martin, B.C. Sales, J. Appl. Phys. 78 (1995) 1013.
[17] S.M. Kauzlarich (Ed.), Chemistry, Structure, and Bonding of Zintl Phases and Ions, VCH Publishers, Inc., New York, 1996.
[18] P.C. Canfield, Z. Fisk, Philos. Mag. B: Phys. Condens. Matter: Stat. Mech. Electron. Opt. Magn. Prop. 65 (1992) 1117.
[19] I.R. Fisher, T.A. Wiener, S.L. Bud'ko, P.C. Canfield, J.Y. Chan, S.M. Kauzlarich, Phys. Rev. B 59 (1999) 13829.
[20] JADE, Materials Data, Inc., 6.1.1 ed., Livermore, CA, 2002.
[21] Crystal Maker for Mac OS X, Ver. 7.1.4, Crystal Maker Software Ltd., Oxfordshire, UK, 2006.
[22] J.A. McCormack, J.P. Fleurial, in: Materials Research Society Symposium Proceedings, vol. 234, 1991, p. 135.
[23] J.W. Vandersande, C. Wood, A. Zoltan, D. Whittenberger, Therm. Cond. 19 (1988) 445.
[24] C. Wood, D. Zoltan, G. Stapfer, Rev. Sci. Instr. 56 (1985) 719.
[25] M. Martinez, G. Brauer, Acta Crystallogr. B B30 (1974) 1083.
[26] A. Bartos, K.P. Lieb, M. Uhrmacher, D. Wiarda, Acta Crystallogr. B 49 (1993) 165.
[27] J.T. Zhao, J.D. Corbett, Inorg. Chem. (1995) 378.
[28] F. Gascoin, S. Ottensmann, D. Stark, S.M. Haile, G.J. Snyder, Adv. Funct. Mater. 15 (2005) 1860.
[29] T. Amano, B.J. Beaudry, K.A. Gschneidner Jr., R. Hartman, C.B. Vining, C.A. Alexander, J. Appl. Phys. 62 (1987) 819.
[30] JPL Materials Device and Technology Group, Online, available: 〈http://www.cco.caltech.edu/~jsnyder/thermoelectrics/〉, 2004.